NASA Technical Memorandum 104276

Water Tunnel Flow Visualization Study of a 4.4% Scale X-31 Forebody

Brent R. Cobleigh and John Del Frate

September 1994

National Aeronautics and
Space Administration

ABSTRACT

A water-tunnel test of a 4.4 percent–scale, forebody-only model of the X-31 aircraft with different forebody strakes and nosebooms has been performed in the Flow Visualization Facility at the NASA Dryden Flight Research Center. The focus of the study was to determine the relative effects of the different configurations on the stability and symmetry of the high-angle-of-attack forebody vortex flow field.

The clean, noseboom-off configuration resisted the development of asymmetries in the primary vortices through 70° angle of attack. The wake of the X-31 flight test noseboom configuration significantly degraded the steadiness of the primary vortex cores and promoted asymmetries. An alternate L-shaped noseboom mounted underneath the forebody had results similar to those seen with the noseboom-off configuration, enabling stable, symmetrical vortices up to 70° angle of attack. The addition of strakes near the radome tip along the waterline increased the primary vortex strength while it simultaneously caused the vortex breakdown location to move forward. Forebody strakes did not appear to significantly reduce the asymmetries in the forebody vortex field in the presence of the flight test noseboom.

NOMENCLATURE

BLS	boundary-layer separation
EFM	enhanced fighter maneuverability
FS	fuselage station, in.
FVF	Flow Visualization Facility
NASA	National Aeronautics and Space Administration
U.S.	United States
α	angle of attack, deg
α_f	flank angle of attack, deg
β	angle of sideslip, deg

INTRODUCTION

The X-31 enhanced fighter maneuverability (EFM) research program is jointly funded by the Advanced Research Projects Agency and the German Federal Ministry of Defense. The flight test portion of the program involves two aircraft and is being conducted by NASA, the U.S. Navy, the U.S. Air Force, Rockwell International, and Deutsche Aerospace at the NASA Dryden Flight Research Center (NASA Dryden). The goals of the flight program are to demonstrate EFM technologies, investigate combat exchange ratios, develop design requirements and databases for future fighter aircraft, and develop and validate low-cost prototype concepts. Figure 1 shows the X-31 flight vehicle.

During the high-angle-of-attack envelope expansion of the two X-31 aircraft, some undesirable flying qualities were discovered at 1 *g* in the lateral–directional axis in the 40° to 60° angle-of-attack region. These characteristics included small to moderate roll and yaw asymmetries; small, random wing drops; and repeatable small, sharp yawing motions. As a group, these behaviors led to maneuver restrictions and a general slowdown of the envelope expansion phase of the flight test program. Forebody aerodynamics were thought to be the primary cause of this high-angle-of-attack behavior.

In an attempt to improve the flying qualities, several boundary-layer transition devices were tested on the forebody and noseboom. The results of those tests have previously been summarized.[1] The transition devices allowed the flight testing to successfully complete the 1-*g* maneuvering envelope expansion of the X-31 aircraft to 70° angle of attack, α.

Shortly into the high-α, elevated-*g* phase of the envelope expansion, a departure from controlled flight occurred on aircraft 2 as the pilot was performing a 2-*g,* split-S maneuver to 60° α. Data analyses showed a large yawing moment that was not modeled in the simulation had triggered this departure. Again, the forebody aerodynamics were suspected to be the cause. An effort was begun to design and test forebody strakes with the goal of improving the forebody vortex symmetry. A wind-tunnel test was conducted in the 30-Ft by 60-Ft Tunnel at the NASA Langley Research Center to refine the strake design and document any changes to the static stability characteristics.[2] The final design was manufactured and installed on both test aircraft.

Shortly before the first flight with the new forebody strakes, a water-tunnel test of a 2.0 percent–scale X-31 model was conducted at the NASA Dryden Flow Visualization Facility (FVF) to examine the general flow characteristics. Limited tests were also run with forebody strakes and without the noseboom. The results showed that the noseboom wake caused the forebody vortex system to become very unsteady and, in some cases, asymmetrical at angles of attack above 40°.

Although the addition of the strakes slightly reduced this unsteadiness, it appeared that the noseboom wake was blanketing the forebody. Even though the results were repeatable, the small model size and resulting lack of geometric detail brought the accuracy of the results into question.

In order to better understand the forebody aerodynamics with differing noseboom and strake configurations, a 4.4 percent–scale model of the X-31 forebody was built for continued testing in the NASA Dryden FVF. The test results were needed in order to make recommendations on what forebody changes should be investigated if the X-31 flight vehicle was unable to achieve its goals with the strake-installed configuration.

WATER-TUNNEL SUITABILITY

Flow visualization in low-speed water tunnels has been an effective method for the analysis of complex flow fields. Although this type of test is conducted at much lower Reynolds numbers than those of flight, there are types of flow which are relatively insensitive to Reynolds number. Phenomena such as vortices and their generation, interaction, and breakdown are in this category and are ideally studied in a facility such as a water tunnel. Erickson concluded that flow fields that are vortex-dominated are similar regardless of Reynolds number.[3] The flow field surrounding the X-31 configuration at high angles of attack can be characterized as vortex-dominated; therefore, Erickson's findings provide confidence that the results from the water-tunnel test are reliable. Erickson also noted that although the water tunnel is not appropriate for obtaining quantitative data about Reynolds number–sensitive effects such as boundary-layer separation (BLS) location, it can be effectively used to evaluate qualitative changes in the flow field caused by changes in aircraft configuration.[3]

MODEL DESCRIPTION

The subject of this test was a 4.4 percent–scale model of the X-31 forebody. Figure 2 shows the model with the N3 noseboom and the S1 strakes installed. Only the forward 40 percent of the flight vehicle was modeled in order to place the largest possible representation of the X-31 forebody in the FVF for maximum fidelity and detail of the model and the resulting flow field. The aft end of the model terminated just aft of the canopy, so the complete forebody, canards, canopy, and inlet were modeled. Although the wing leading-edge strakes come forward of the aft end of the canopy on the full-scale aircraft, the lack of the wing and aft fuselage on the model would have corrupted any effect of the strakes. Thus, the leading-edge strakes were not included on the model.

The model was fabricated by stacking brass templates of the fuselage cross sections every 0.44 in. and sandwiching high-density styrofoam between the templates. Brass alignment rods were used to hold all of the pieces together. The foam was then shaped flush with the templates. The model was covered using a very thin coating of fiberglass cloth and epoxy and was painted white. The forebody was marked with fuselage station, *FS*, reference lines every 10 full-scale inches. The nose tip of the aircraft was located at *FS* –20. Stainless steel tubes with a 0.024 in. inner diameter were installed through the aft end of the model. These tubes carried the different colors of dye and exited at the dye port locations shown in figure 3.

The canard was adjustable from outside of the water tunnel using an internal bell crank–style adjusting device. All of the nosebooms tested had dye-carrying capability, which allowed investigation of the noseboom wake. The lower lip of the engine inlet was drooped 26° to duplicate the X-31 high-α configuration. A mass flow meter regulated the flow through the inlet.

Results from seven X-31 model configurations tested in the FVF are presented. Table 1 shows the components tested on each of the configurations. Figure 4 shows sketches of each of the strakes and nosebooms and includes some basic dimensions. All dimensions given in this paper refer to full-scale aircraft unless otherwise specified.

DESIGN OF STRAKES AND NOSEBOOMS

The strake designs tested in this investigation originated from a wind-tunnel test in the 30-Ft by 60-Ft Tunnel at the NASA Langley Research Center.[1] The purpose of the wind-tunnel test was to design a strake that would minimize the forebody yawing asymmetries without adversely affecting the static rolling, yawing, and pitching moment characteristics. Many strake

designs were evaluated using this criterion. These designs included the S1 and S2 strakes (fig. 4) as well as 1.2 in.–wide strakes. All of the strakes that were installed horizontally along the aircraft waterline succeeded in reducing the static yawing moment asymmetry throughout the angle-of-attack range. The S1 strakes were the minimum length that fulfilled the design requirements. When the S1 strake was increased in length (for example, the S2 strake), a noseup pitching moment penalty was encountered. As a result of the wind-tunnel test, the S1 strake was installed on both X-31 aircraft for flight testing.

A previous 2.0 percent–scale X-31 water-tunnel test had shown that the flight test noseboom wake had a significant effect on the forebody vortex stability. This effect was caused by the placement of the noseboom under the forebody resulting in the noseboom wake directly interacting with the primary vortices at high angles of attack. Several nosebooms were designed for testing in the water tunnel to study this effect further and try to minimize the interaction between the noseboom flow and the forebody vortex system without requiring a major aircraft modification. In addition to the flight test noseboom, N1, figure 4 shows a chin-mounted, L-shaped noseboom, N2, and a nose tip–mounted noseboom, N3. All of these nosebooms were acceptable because of their ease of fabrication and installation on the aircraft. A diameter of 2.5 in. was used for the N2 and N3 nosebooms.

FLOW VISUALIZATION TECHNIQUE

The NASA Dryden FVF is a closed-return type water tunnel with a vertical test section (fig. 5). Testing in the FVF is typically performed at a rate of approximately 3 in/sec. At this speed, the velocity profile can vary approximately $\pm$0.18 in/sec, and the turbulence intensity level is less than 1 percent. A detailed description of the facility has previously been given.[4]

The dye tracer technique was used in this test. This technique consists of emitting dye that is entrained in the flow field of interest, thereby revealing the flow structure to the observer. Two- and three-dimensional flow structures surrounding a body can be observed and analyzed in the FVF using this technique.

Dye was supplied to the X-31 model while it was mounted in the test section through lines that were connected to pressurized dye containers located outside of the test section. The X-31 model was fabricated with internal dye lines that led to flush ports on the model surface from which the dye entered the flow field. The dye flow rate from each pressurized dye container was regulated using a needle valve. The dye flow was adjusted to provide enough dye to visualize the local flow field without affecting it.

TEST CONFIGURATIONS

Configuration A was representative of the original X-31 flight test vehicle, which included a large diameter (3.5 in.) noseboom, N1, mounted on the underside of the forebody near *FS* 40. The nose tip was kept pointed. This configuration was flown in the flight test program on ship 1 for flights 1 to 96 and on ship 2 for flights 1 to 77.

Configuration B was the same as configuration A except that the noseboom was removed.

Configuration C was modified from configuration B by adding S1 strakes on the sides of the forebody, starting just aft of the nose tip. The strake dimensions were 0.60 in. wide by 20 in. long. Configurations C through F also had a rounded, 0.60 in.–radius nose tip.

Configuration D had the baseline strakes, S1, and the large diameter noseboom, N1. This configuration was flown in the flight test program on ship 1 for flights 97 to present flights and on ship 2 for flights 78 to 91 and flights 95 to 132.

Configuration E used the extended forebody strakes, S2, and the N1 noseboom. This configuration was flown on ship 2 for flights 92 to 94.

Configuration F was modified from configuration C by installing an L-shaped noseboom, N2, at *FS* 50. The L-shaped noseboom was 60 in. long and had a diameter of 2.5 in.

Configuration G retained the shorter forebody strakes, S1; however, a nose tip–mounted noseboom, N3, was installed and the strakes were faired into the sides of the noseboom. The N3 noseboom was 48 in. long and had a diameter of 2.5 in.

TEST CONDITIONS AND PROCEDURES

The majority of the tests were conducted at a tunnel velocity of 3 in/sec. This velocity corresponds to a Reynolds number of 3080 when based on a model forebody diameter of 1.6 in. at the canopy leading edge.

Past experience has shown this velocity to be an appropriate setting for good flow visualization. Prior to taking data at each condition, the flow was allowed to stabilize for approximately 2 min.

During the tests, the angle of attack and the yaw angle, which is also referred to as flank angle of attack, were varied. The sideslip angle, β, is related to the flank angle of attack by the equation

$$\beta = \text{atan}\,[\tan(\alpha_f)\cos(\alpha)]$$

where α_f is the flank angle of attack. Notes, videotape, and still photographs were taken at angles of attack of 20°, 30°, 35°, 40°, 45°, 50°, 55°, 60°, 65°, and 70° for each of the configurations tested. In addition, several of the configurations were tested with flank-angle-of-attack values of –10°, –5°, 0°, 5°, and 10° at angles of attack of 45°, 55°, and 65°. Prior to testing each of the configurations, the yaw angle of the model was aligned with a calibration rig, and the pitch and roll angles were adjusted using a level.

Because the emphasis of the water-tunnel test was on the relative changes in the forebody flow field with different nosebooms and strakes, other variables were either kept constant or scheduled as a function of the angle of attack. Figure 6 shows an approximation to the actual flight test canard schedule used. The canard was aligned with the freestream flow up to 45° α, after which it was fixed at a 45° deflection. In order to maximize air intake, the inlet lip was fixed at –26° for all of the test conditions, which corresponds to the full-down, high-α position. The inlet mass flow ratio was adjusted to approximately 1.0, which equates the velocity through the inlet to the freestream tunnel velocity. The water pressure in the FVF test section forced water through the model inlet and was then adjusted using a valve outside of the test section. Adjustments of the mass flow were found to slightly alter the primary vortex breakdown location; however, this effect was of minor concern.

RESULTS AND DISCUSSION

The flow characteristics of each of the forebody configurations are described in the first subsection. The general canard flow field, which was similar for each of the configurations, is discussed second. In the third subsection, a comparison of the configurations illustrates the relative effects of the various noseboom and strake changes, with particular attention paid to vortex asymmetries, vortex breakdown, BLS, and flow-field stability.

Forebody Flow Field

The following sub-subsections detail the flow characteristics of each forebody configuration.

Configuration A: N1 Noseboom, No Strake

Configuration A was representative of the original X-31 flight test vehicle forebody, having a large diameter noseboom, N1, and no forebody strakes. At 20° α, the flow over the X-31 forebody was attached and laminar (fig.7). At 30° α, the flow was beginning to separate from the forebody; however, the flow remained laminar (fig. 8). The flow over the noseboom was laminar and steady as it traveled into the forebody flow field. The primary forebody vortices, although weak, started to form at approximately 35° α (fig. 9). The benign effect of the noseboom ended as the model reached 40° α. At this condition, an eddy developed between the noseboom and forebody (fig. 10). In addition to the eddy, a periodic flow disturbance alternated from each side of the noseboom. This disturbance caused the primary vortices to oscillate at the same frequency. As the angle of attack reached 50°, the primary vortices increased in strength while still subject to the periodic flow from the noseboom (fig. 11). The forebody flow disturbances became more random at this condition.

Figure 12 shows that at 55° α, the primary vortices started to show a slight asymmetry. The right vortex core is higher off the body and slightly more outboard from the model centerline than the left vortex is. Another asymmetrical feature of the flow field was the vortex core breakdown, which occurred further aft on the right vortex. In addition, the BLS line occurred earlier (lower) on the right side of the forebody. Because the unsteadiness in the flow field renders the other features of the flow asymmetry in figure 12 not easily discernible, a generic sketch of the asymmetrical flow condition on the model is shown in figure 13. As shown, the resulting vortex-induced side force on the forebody is in the direction of the lower vortex. This side force is caused by the increased amount of suction provided by the boundary layer, which is attached over a larger forebody area than the opposite forebody side, and the high vortex velocity near the model surface.

As the angle of attack increased to 60°, the flow asymmetry switched sides. The right vortex became the lower vortex and moved inboard nearly to the centerline (fig. 14). The left vortex moved high and away from the model centerline. The difference in vortex heights and the amount of deflection in the vortex paths at 60° α (fig. 14(a)) suggest that the magnitude of the asymmetry is greater than the magnitude at 55° α. Once again, the higher vortex resisted breakdown until further downstream. The BLS occurred significantly earlier on the left side of the forebody, again corresponding to the higher, more outboard vortex. Notes and videotape indicate that vortex symmetry was restored as the model approached 65° α; however, the flow continued to have a large unsteady component. Although the primary vortex breakdown location moved forward of the canopy at 70° α (fig. 15), the vortex cores remained symmetrical.

Configuration B: No Noseboom, No Strakes

Configuration B was the clean forebody with no noseboom or forebody strake. With the removal of the N1 noseboom, the primary vortices started to form at a lower angle of attack than they had with the noseboom-on configurations. Figure 16 shows that the vortices had formed by 30° α. From 40° to 50° α, the forebody flow field was steady and symmetrical (figs. 17 and 18). Figure 19(a) shows that with the noseboom off, the primary vortex cores are at an equal distance above the forebody surface at 55° α. This flow symmetry is in contrast to the asymmetry observed at the same conditions with configuration A (fig. 12).

From 35° to 70° α, the primary vortices remained very symmetrical, as shown at 40°, 50°, 55°, and 65° α in figures 17, 18, 19(b), and 20. The increase in strength of the primary vortices accompanying increasing angle of attack can be observed by noting the reduction in distance between consecutive vortex rotations. These stronger vortices have a sharper helix angle than those seen at lesser angles of attack because of their higher rotational velocity.[5] A comparison of the results shown in figures 21 and 14(a) reveals that, unlike the noseboom-on example, the unsteady flow field component forward of the canard was absent from the forebody flow field. This steadiness of the flow field forward of the canard was seen over the entire angle of attack range for this configuration. The vortices remained symmetrical and stable to 70° α.

Unlike configuration A, which had the N1 noseboom installed, configuration B had no asymmetries in the primary vortex cores throughout the angle-of-attack range tested. No other configuration tested yielded the uniformity and steadiness in the flow observed with this configuration.

Configuration C: No Noseboom, S1 Strake

Configuration C consisted of the X-31 model with the longitudinal S1 forebody strakes installed and a nose tip that was rounded to a 0.60 in. radius. Formation of the primary vortices initiated along the strake at 30° α (fig. 22). From 35° to 50° α, the primary vortices gained in strength while staying symmetrical. This symmetry was evidenced by the tightly wound vortex core at 40° α (fig. 23), which was not present without the strake (fig. 17). Stable symmetrical vortices were also observed at 50° α (fig. 24). The forward movement of the primary vortex breakdown location with increasing angle of attack is clearly shown by comparing figures 23 and 24. A small difference in the longitudinal breakdown location occurred at 55° α (fig. 25(a)), although the vortex paths were at the same distance above the forebody (fig. 25(b)). A smaller, but noticeable, difference in the primary vortex breakdown location was also seen at 60° α (fig. 26). Some unsteadiness in the flow field was noticed above 55° α, but not as much as was seen in the presence of the N1 noseboom. The primary vortex breakdown symmetry was restored at 65° α (fig. 27). The vortex symmetry remained through 70° α.

Configuration D: N1 Noseboom, S1 Strake

Configuration D included the N1 noseboom and the S1 strake in addition to the rounded nose tip. This configuration matched the flight test aircraft configuration after the aircraft was modified with strakes. The flow field around the forebody below 40° α was similar to the strake-on, noseboom-off configuration C. At and above 40° α, the flow around the noseboom caused the primary vortices to become unsteady, although the symmetry in the flow was not altered (fig. 28). The effect of the noseboom addition can be seen by comparing this configuration at 40° α to the same condition with the noseboom removed (fig. 23). The unsteadiness appears as a random component in the streamlines and vortex cores with the noseboom on. This unsteadiness

increased with angle of attack and by 55° α, the primary vortices became asymmetrical as shown in figure 29. Both vortices were shifted to the right with respect to their symmetrical position, with the left vortex lower than the right vortex. The left vortex broke down at the canopy leading edge while the right remained intact for approximately 20 in. further downstream. The BLS occurred earlier on the right side of the forebody.

At 60° α, the vortex asymmetry switched, the right vortex now moving low and inboard and the left vortex moving high and away from the centerline (fig. 30). As expected, the vortex breakdown occurred further forward on the right side and the BLS occurred lower on the left side of the forebody. The symmetry of the vortex system was restored between 65° and 70° α, although the unsteadiness of the flow field remained. At and above 50° α, a significant flow interaction between the noseboom and the forebody existed. Flow traveling forward from the attachment point of the noseboom met flow traveling aft from the forward portion of the boom and then traversed into the forebody vortex field (fig. 29(a)). Notes and videotape showed that this behavior continued up to 70° α.

Configuration E: N1 Noseboom, S2 Strake

Configuration E included the extended strakes, S2; the flight test noseboom, N1; and the rounded nose tip. As with previous strake-on configurations, the primary vortices started to form at 30° α, increasing in strength as angle of attack increased. The unsteady forebody flow field caused by the noseboom developed at approximately 35° α (fig. 31). The extreme unsteadiness of the flow field made analyses difficult. Symmetry in the vortex cores was noted up to 45° α. The typical noseboom-on asymmetry, seen in configurations A and D at 55° α, started at 50° α. The asymmetrical flow patterns, though, were the same as those seen previously. The left vortex moved lower and toward the centerline, and the right vortex moved high and away. The right vortex breakdown occurred further aft on the model, and the boundary layer on the right side of the forebody separated earlier. Figure 32 shows a sketch of the vortex paths and breakdown locations.

At 55° α, the vortex asymmetry switched sides. Figure 33 shows that the right vortex tracked closer to the centerline. The symmetrical flow field was restored at 60° α and above. The effect of the S2 strake, relative to the S1 strake or plain forebody configurations, was to reduce the asymmetry onset angle of attack. Thus, the S2 strake did not improve the forebody vortex flow field relative to the S1 strake.

Configuration F: N2 Noseboom, S1 Strake

Configuration F included an alternate noseboom that was designed with the goal of minimizing the effect of the noseboom wake on the forebody vortical flow. This L-shaped noseboom, N2, was mounted under the forebody near *FS* 50 (fig. 34). The baseline S1 strake and rounded nose tip were also installed on configuration F.

A concern was that this noseboom might feed vortical flow into the engine inlet at high angles of attack where the stall margins of the engine are reduced. Above 20° α, the flow over the noseboom missed the inlet and traveled around the fuselage (fig. 34). At lower angles of attack, the wake of the noseboom did enter the inlet.

The primary vortices formed at 30° α, as they had previously with the S1 strake. Although previous tests showed that the flight test noseboom, N1, triggered flow unsteadiness throughout the forebody flow field at and above 40° α, this effect was not found with the N2 noseboom. A comparison at 40° α between the N1 and N2 nosebooms (figs. 28 and 35) shows that the forebody flow field with the N2 noseboom installed had no unsteady components in the primary vortices. As the angle of attack was increased above 40°, the primary vortices continued to remain symmetrical and stable. A comparison of figures 25(b), 29(a), and 36 shows that the forebody flow field with the N2 noseboom installed more closely matched the flow field of the configuration without a noseboom than the unsteady flow field caused by the N1 noseboom.

Vortex shedding from the noseboom was first noticed at 60° α (fig. 37). This vortex shedding did not affect the symmetry or stability of the vortex flow field. In addition to the vortex shedding, a slowly rotating eddy developed between the noseboom and forebody at and above 60° α (fig. 37). Figure 38 shows that the addition of the N2 noseboom appeared to eliminate the uneven left and right vortex breakdown observed at 55° α in configurations without nosebooms. The wake of the N2 noseboom entered into the forebody flow field between *FS* 15 and *FS* 60 at approximately 65° α (fig. 38); however, the primary vortices remained stable and symmetrical. Some minor flow field unsteadiness was observed at 70° α; however, the primary vortices remained symmetrical.

Configuration G: N3 Noseboom, S1 Strake

Configuration G included a noseboom similar in design to that flown during the X-29A (Grumman Aerospace Corporation, Bethpage, New York) high-α flight test program.[6] Figures 39 and 40 show the N3 noseboom mounted at the apex of the radome with the S1 forebody strakes blended into the side. As the photographs were analyzed, it was noticed that the noseboom had been offset slightly to the right during these tests.

The primary vortices developed in a fashion similar to the noseboom-off test (configuration C). A comparison of the flow field in the presence of the N3 noseboom (fig. 39) with the noseboom-off configuration (fig. 23) shows a similar vortex pattern at 40° α. Although flow from the noseboom is clearly feeding into the vortex cores in figure 39, no unsteadiness was noted. In all of the photographs above 30° α, the primary vortex pair was shifted slightly to the right side of the forebody. Because this shift was not seen for the other configurations with the S1 strake, it is likely that this shift was caused by the slight noseboom misalignment during the test. Through 45° α, the vortices strengthened and remained symmetrical (except for the slight shift to the right).

At 50° α, the wake from the noseboom was vortical in nature and was being drawn into the forebody vortex system (fig. 40). This vortical wake may have been responsible for a difference in the left and right vortex breakdown locations. The left vortex broke down approximately 10 in. forward of the right vortex, although no difference in height above the model surface was noticed. The asymmetrical breakdown of the primary vortices was not discernible in the photographs; therefore, only notes and videotape could be used. This asymmetrical breakdown of the primary vortices continued through 60° α as the unsteadiness in the forebody flow field increased. The noseboom wake continued to feed into the vortices throughout this angle-of-attack range. Above 60° α, the vortices became more unsteady with increasing angles of attack, but the breakdown location of the primary vortices became nearly symmetrical.

Canard Influence

Although the canard was aligned with the freestream flow up to 45° α (fig. 6), the local canard angle of attack was not 0°. It has been documented that the forebody induces an upwash effect on the surface flow at high angles of attack.[7, 8] Although flow visualization tests were not performed for the outboard portion of the canard, the inboard section was subject to this forebody upwash effect. The dye flow from the port located forward of the canard at *FS* 31 (fig. 2(a)) was used to measure the upwash angle on the photographs as the streamline crossed the waterline which passes through the canard rotation point. The difference between the surface flow angle and the canard angle was used to approximate the local inboard canard angle of attack.

Below 45° α, the canard had a nearly constant, nonzero local angle of attack (fig. 41). At 20° α (fig. 7), the low pressure area over the top of the canard turned the forebody surface flow downward. The streamlines converged near the canard trailing edge. At 30° α (fig. 8), a flow pattern similar to a Karman vortex street started to form aft of the canard trailing edge. This flow-field condition continued to higher angles of attack (fig. 42). The wake behind the canard was fully stalled at 55° α (fig 12). Since the local canard angle of attack increases almost linearly with the model angle of attack above 45° α, the canard remained fully stalled at angles of attack above 55°.

In general, the onset of the canard stall was observed to coincide with a slight increase in instability of the forebody vortex cores at the point of their intersection with the canard wake and aft. This instability promoted premature vortex breakdown with increasing angles of attack, which will be covered in the next subsection.

Comparison of Configurations

Because the X-31 model consisted of a forebody only, the absolute value of some of the data taken (such as vortex breakdown location) is of less importance than the relative changes in the flow field between the strake and noseboom configuration changes. These relative differences were considered to be the most important information obtained from the test series. Comparisons between configurations include vortex symmetry, vortex breakdown location, flow-field stability, and BLS. Vortex symmetry was defined with respect to the centering of the vortex pair around the model centerline and the relative distance of the individual vortex cores from the forebody along their trajectories. Vortex breakdown location was given as the longitudinal position at which the diameter of the vortex cores increased rapidly and the rotational velocity simultaneously decreased. Flow-field stability

consisted of the presence or lack of oscillations or random unsteadiness. The BLS line was defined as the position along the forebody where the dye flow left the model surface.

Primary Vortex Asymmetry

One of the main goals of the water-tunnel investigation was to look for the tendency of the primary vortex cores to become asymmetrical with various noseboom and strake changes. Asymmetry of the vortex cores with respect to the model centerline and height above the forebody surface was noted on configurations A, D, and E. These configurations had only one common element, which was the flight test noseboom, N1. Unfortunately, the unsteady wake of the N1 noseboom also makes it difficult to visualize the asymmetry in the still photographs. Thus, notes and videotape were used extensively for this analysis.

The development of the asymmetry with the N1 noseboom installed was similar for each of the forebody configurations (fig. 13). Typically, the left vortex moved low and inboard toward the model centerline and the right vortex moved high and away from the centerline at a specific angle of attack. This movement was followed by a switch in the positions as the model angle of attack was increased by 5°. The lower vortex tended to break down about 10 to 20 full-scale inches forward of the higher vortex. The BLS line was lower on the side of the forebody that had the higher, more outboard vortex.

The onset angle of attack of the asymmetry with the N1 noseboom was affected by the strake configuration. With the S1 strake or no strake installed, the first asymmetry started at 55° α. The extended strake, S2, caused this asymmetry to occur at 50° α.

The L-shaped noseboom, N2, showed no tendency to cause the vortices to become asymmetrical at high angles of attack. The nose tip–mounted noseboom, N3, showed a slight tendency of the vortex cores to break down asymmetrically between 50° and 60° α.

Primary Vortex Breakdown

The longitudinal position of the vortex breakdown location was directly affected by the installation of strakes on the model. Comparing figures 26 and 21 illustrates the change in the primary vortex breakdown location with the addition of the S1 strakes for the 60° α test condition. Figure 43 shows the longitudinal breakdown location of the primary vortices as a function of angle of attack, with and without the S1 strakes. As stated earlier, the S1 strake significantly increased the rotational velocity in the primary vortex cores. The increased rotational velocity required a smaller adverse pressure gradient downstream to induce breakdown.[9] As a result, the addition of the strakes shifted the primary vortex breakdown location forward at a given angle of attack.

Figure 43 also shows the change in slope of the graph for both configurations at 50° α. Above 50° α, the vortex breakdown location moved further forward with a given amount of angle-of-attack change. This change in slope correlates with the onset of canard stall. The canard schedule froze the canard at 45° as the model moved above 45° α (fig. 6). This canard schedule, combined with the fuselage upwash effect described previously, caused the canard to stall by 55° α. Canard stall produced the adverse pressure field downstream of the vortex path that caused the earlier breakdown.

Flow-Field Stability

Another important component of the forebody flow field was the stability of the vortices. Up to 40° α, all of the configurations had laminar, stable flow throughout the forebody area, excluding the canard trailing edge wake. Above this angle of attack, many of the configurations had unsteady or oscillatory flow. The clean forebody model without strakes showed no tendency to become unsteady or oscillatory. As the primary vortices formed, their paths remained stationary with respect to the X-31 model, with and without strakes. The flight test noseboom, N1, created an oscillating wake that entered and altered the forebody flow field.

Figures 18 and 24 show that the vortex cores run symmetrically over the forebody in a stationary position for noseboom-off configurations at 50° α, but adding the noseboom (fig. 11) introduced random components to the flow field that affected the vortex path. The L-shaped noseboom, N2, was designed so that its wake would not intersect with the forward portion of the forebody. This design proved successful in reducing the wake influence through 65° α, although some unsteadiness in the flow field was observed at 70° α. The nose tip–mounted noseboom, N3, produced some unsteady flow disturbances above 55° α, though of much smaller magnitude than the N1 noseboom produced.

Boundary-Layer Separation

The primary BLS line was observed on the forebody of the model by noting the location where the dye left the model surface. An adequate amount of dye was available for visualizing the separation line up to approximately 60° α. Although the water tunnel has not been established as an accurate tool in the prediction of the separation line position on forebodies at high angles of attack because of low Reynolds number effects,[3] the relative differences in the separation line were analyzed to establish general trends with configuration changes.

Figure 44 shows a comparison of the separation line with S1 strakes, S2 strakes, and no strakes at angles of attack of 35°, 45°, and 55°. The data plotted are projections of the separation line on the vertical plane measured from photographs of the left side view. As expected, BLS occurred at the strake edge, which was 5 in. below the zero waterline. Aft of the strake, the separation line curved sharply up and asymptotically approached the same separation line as that of the forebody without strakes at 35° and 45° α. At these angles of attack, the separation lines with and without the strake were nearly identical at a point 20 in. aft of each strake aft end. As previously described, all configurations with the N1 noseboom installed had asymmetries in the BLS between the left and right sides at 55° α. With the S1 strake, the left side BLS was higher than the right. With the S2 strake, the right side BLS was higher than the left at 55° α. Figure 44 shows that, as a result, the S1 strake separation line is slightly higher and the S2 strake is lower than the strake-off separation line at this condition.

CONCLUDING REMARKS

A water-tunnel study of a 4.4 percent–scale forebody model of the X-31 aircraft was conducted in the Flow Visualization Facility at the NASA Dryden Flight Research Center. The primary focus of the study was the investigation of the effects of various combinations of nosebooms and strakes on the high-angle-of-attack forebody flow field. Particular attention was paid to the development or reduction of asymmetries and unsteadiness with the different configurations.

The most important findings were as follows:

- The X-31 model without a noseboom or strakes installed had stable, symmetrical forebody vortices through 70° angle of attack, α.
- With the addition of the flight test noseboom, N1, the flow field became unsteady and oscillatory at and above 40° α. The N1 noseboom addition also correlated with the development of asymmetrical primary vortices. The onset of the asymmetry was at 55° α with no strake or the S1 strake and decreased to 50° α with the longer S2 strake.
- Adding strakes to the forebody increased the strength of the vortex cores and resulted in earlier vortex core breakdown.
- Adding strakes did not significantly reduce the tendency of the noseboom influence to cause asymmetries.
- The extended strakes, S2, did not show a significant improvement in flow-field symmetry relative to the S1 strakes.
- The L-shaped noseboom, N2, allowed the flow field to remain stable and symmetrical up to 65° α. Some minor flow-field unsteadiness was observed at approximately 70° α.
- The nose tip–mounted noseboom, N3, delayed the onset of flow-field unsteadiness to a higher angle of attack. Although the vortex pair remained nearly symmetrical with respect to the model centerline, some asymmetry in the vortex breakdown was noted between 50° and 60° α.

As observed in this study, the wake of the flight test noseboom plays an important role in the development of the primary vortices at high angles of attack. The effect is not nullified with the application of strakes on the forebody. The L-shaped noseboom, N2, combined with the basic S1 strake appears to be the best combination to minimize the high-angle-of-attack asymmetries and reduce unsteady, oscillating flow disturbances.

Dryden Flight Research Center
National Aeronautics and Space Administration
Edwards, California, August 29, 1994

ACKNOWLEDGMENTS

Special thanks is owed to Daniel Garrabrant for his craftsmanship and endless patience in building and modifying the X-31 model.

REFERENCES

[1]Cobleigh, Brent R., "High-Angle-of-Attack Yawing Moment Asymmetry of the X-31 Aircraft from Flight Test," AIAA-94-1803, June 1994.

[2]Croom, Mark A., Fratello, David J., Whipple, Raymond D., O'Rourke, Matthew J., and Trilling, Todd W., "Dynamic Model Testing of the X-31 Configuration for High-Angle-of-Attack Flight Dynamics Research," AIAA-93-3674 CP, Aug. 1993.

[3]Erickson, Gary E., *Vortex Flow Correlation*, AFWAL-TR-80-3143, Jan. 1981.

[4]Del Frate, John, *NASA Dryden Flight Research Center, Flow Visualization Facility*, NASA TM-4631, 1994.

[5]Payne, Francis M., *The Structure of Leading Edge Vortex Flows Including Vortex Breakdown*, University of Notre Dame, May 1987.

[6]Fisher, David F., Richwine, David M., and Landers, Stephen, *Correlation of Forebody Pressures and Aircraft Yawing Moments on the X-29A Aircraft at High Angles of Attack,* NASA TM-4417, 1992.

[7]Keener, Earl R., *Flow-Separation Patterns on Symmetric Forebodies*, NASA TM-86016, 1986.

[8]Fisher, David F., Richwine, David M., and Banks, Daniel W., *Surface Flow Visualization of Separated Flows on the Forebody of an F-18 Aircraft and Wind-Tunnel Model*, NASA TM-100436, 1988.

[9]Wedemeyer, E., "Vortex Breakdown," *High Angle of Attack Aerodynamics*, AGARD-LS-121, Mar. 1982, pp. 9-1–9-17.

Table 1. The X-31 model configurations.

	Component	Configuration						
		A	B	C	D	E	F	G
Nosebooms	Flight test noseboom, N1	X		X	X			
	L-shaped noseboom, N2						X	
	Nose tip noseboom, N3							X
Strakes	Short Strake, S1			X	X		X	X
	Extended strake, S2					X		
Nose tip shapes	Rounded nose tip (0.6 in. radius)			X	X	X	X	
	Sharp tip	X	X					

EC92-09164-1

Figure 1. The X-31 flight vehicle.

(a) The model.

Figure 2. The 4.4 percent–scale X-31 forebody model.

(b) Front view.

(c) Side view.

Figure 2. Concluded.

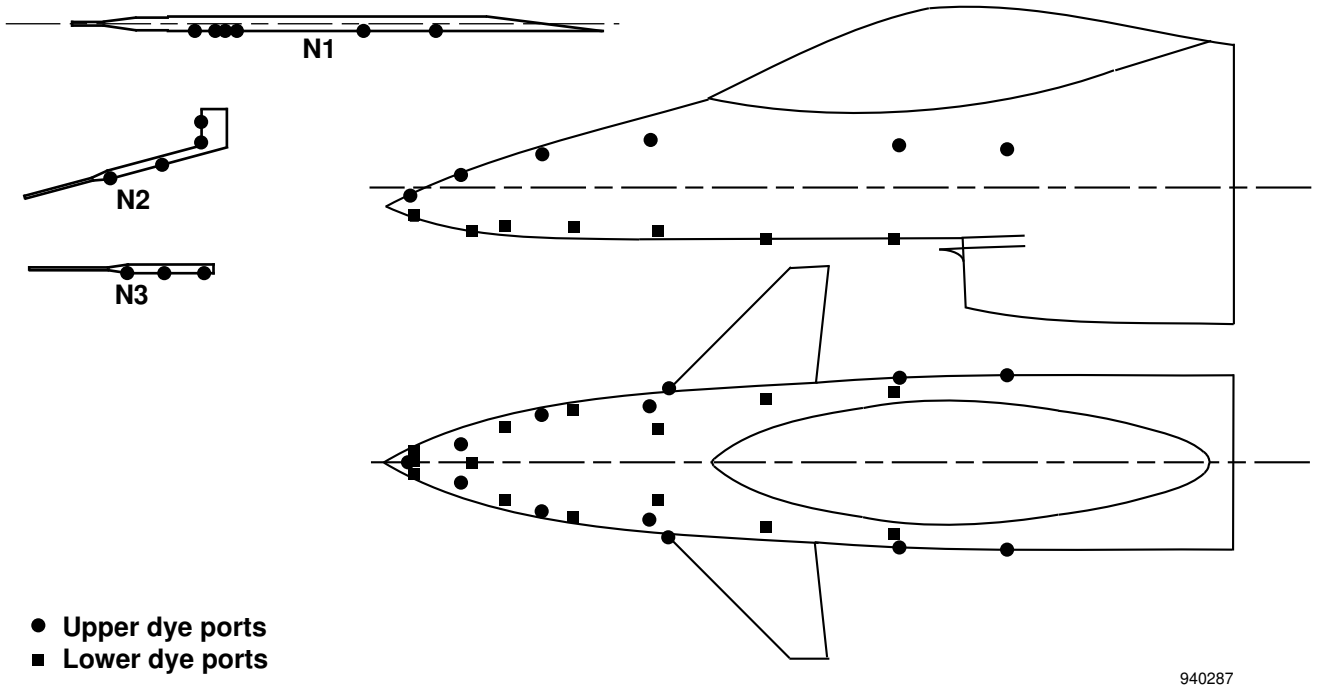

Figure 3. Model dye port locations.

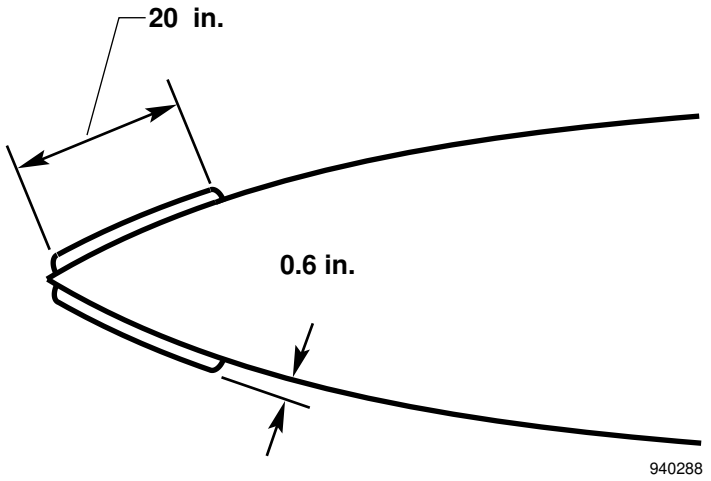

(a) S1 strake (top view).

Figure 4. Nosebooms and strakes tested.

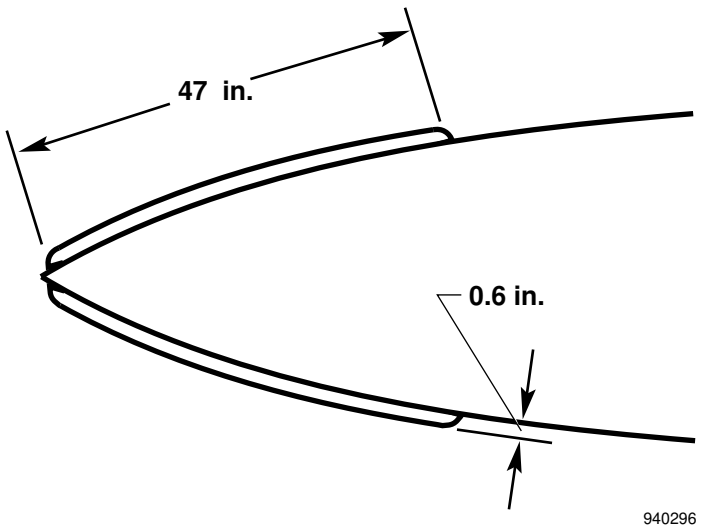

(b) S2 strake (top view).

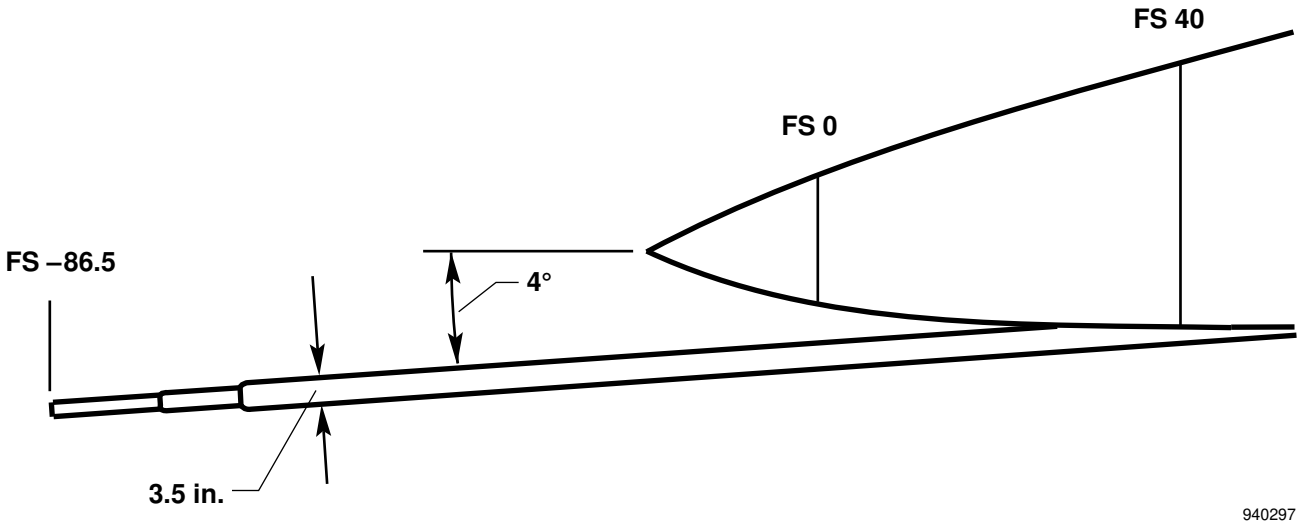

(c) N1 noseboom (side view).

Figure 4. Continued.

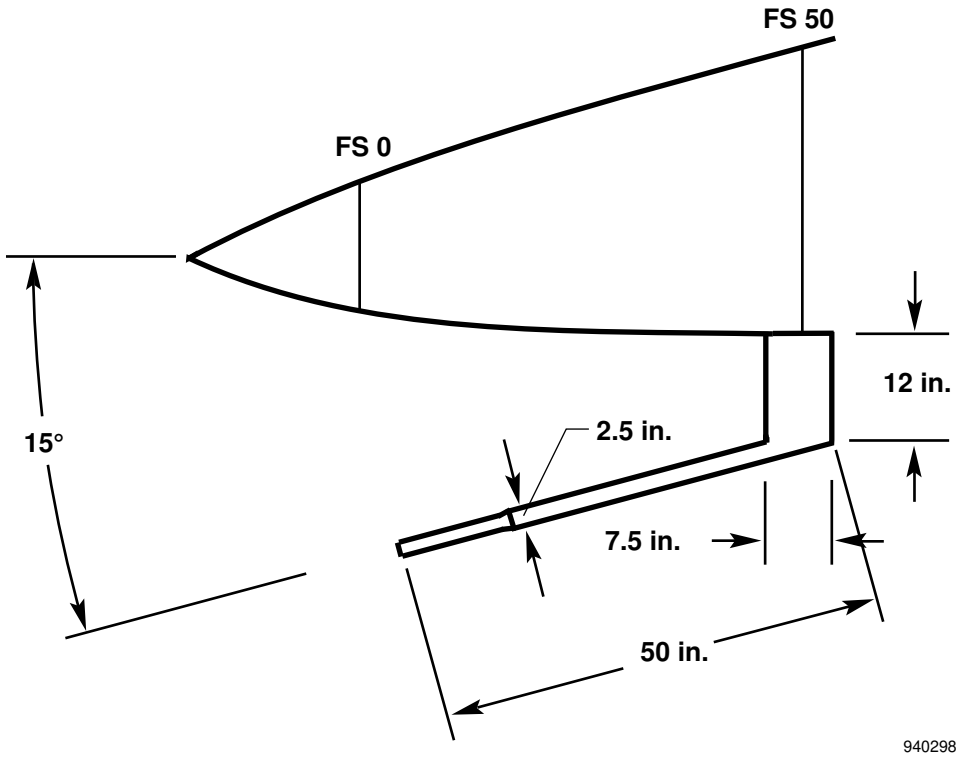

(d) N2 noseboom (side view)

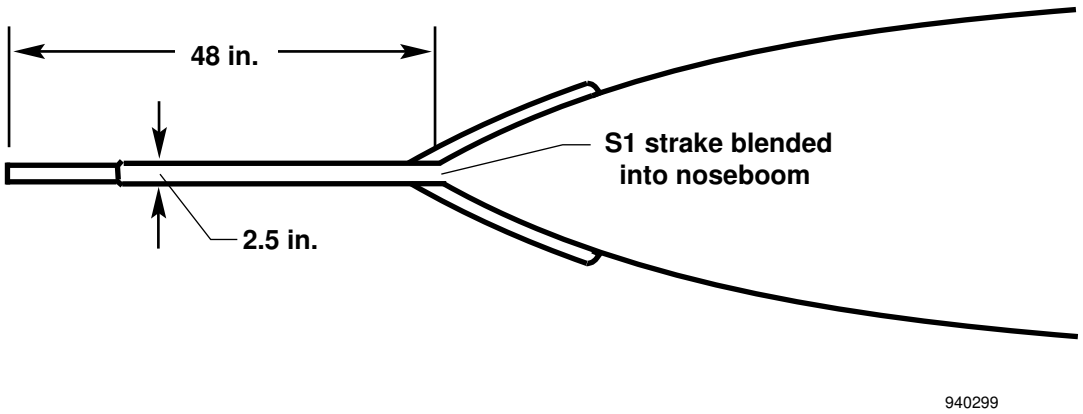

(e) N3 noseboom (top view).

Figure 4. Concluded.

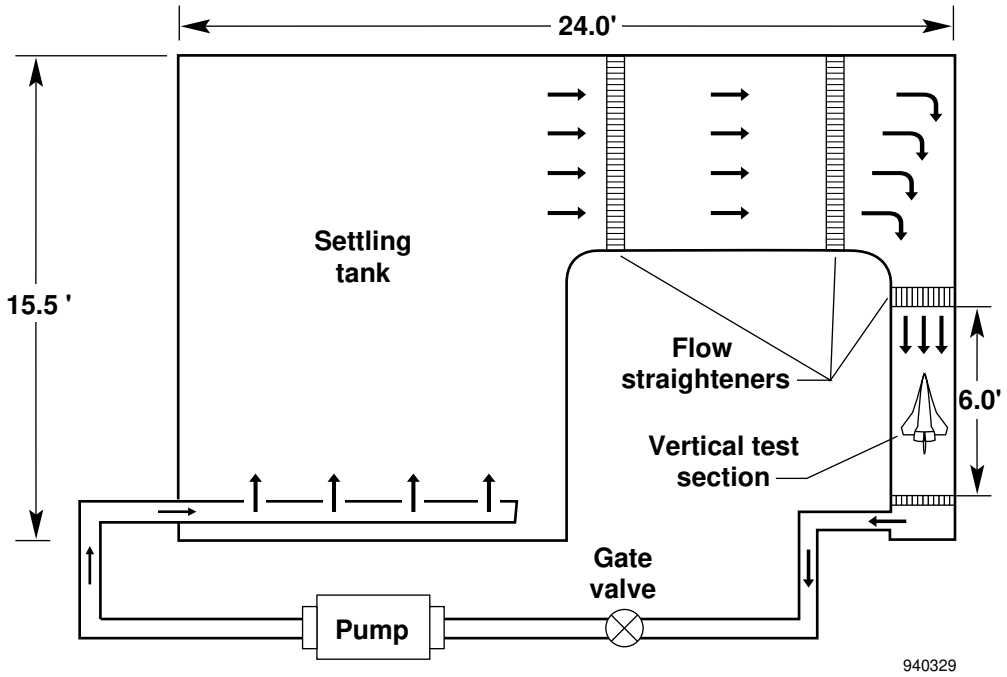

Figure 5. The Flow Visualization Facility.

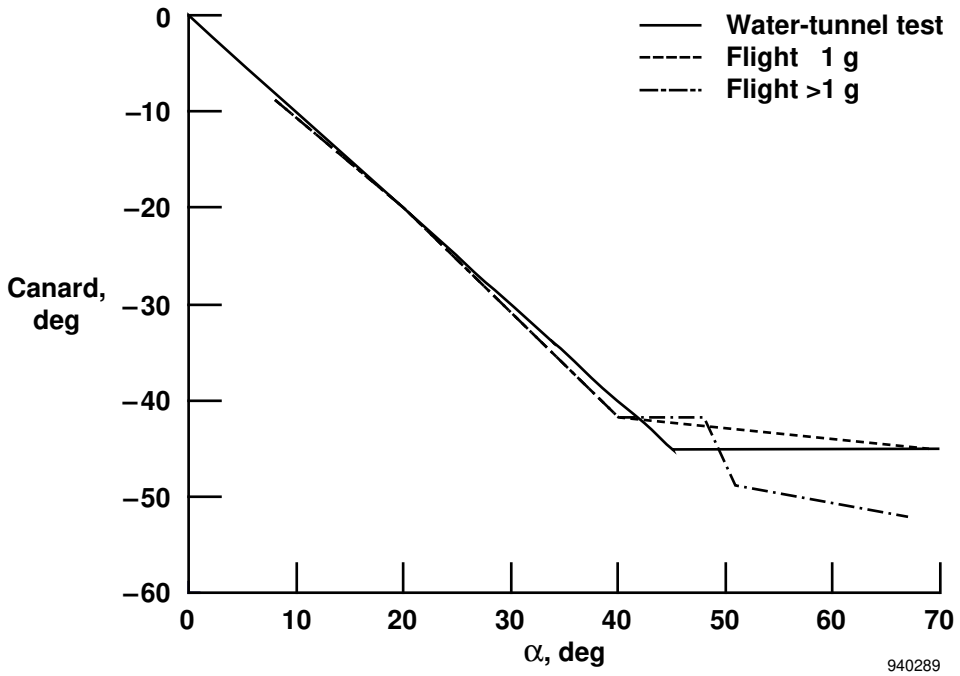

Figure 6. Canard deflection schedule.

Figure 7. Configuration A at 20° angle of attack (side view).

Figure 8. Configuration A at 30° angle of attack (side view).

Figure 9. Configuration A at 35° angle of attack (top view).

Figure 10. Configuration A at 40° angle of attack (side view).

Figure 11. Configuration A at 50° angle of attack (top view).

Figure 12. Configuration A at 55° angle of attack (side view).

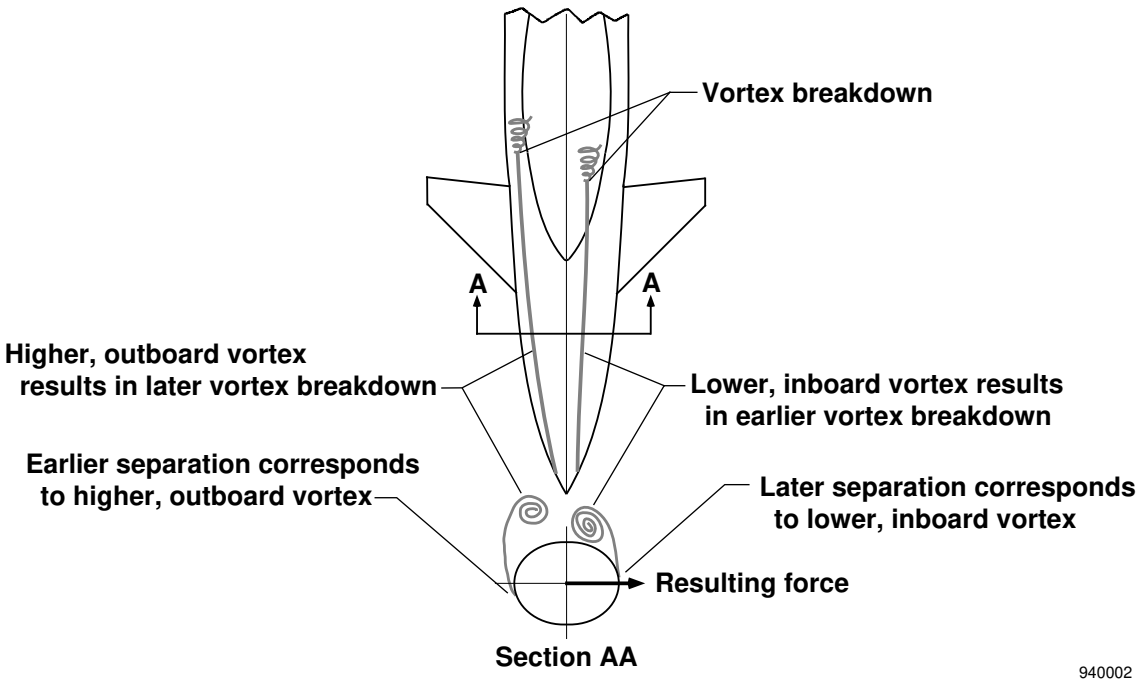

Figure 13. Generic flow asymmetry.

(a) Side view.

Figure 14. Configuration A at 60° angle of attack.

(b) Top view.
Figure 14. Concluded.

Figure 15. Configuration A at 70° angle of attack (side view).

Figure 16. Configuration B at 30° angle of attack (top view).

Figure 17. Configuration B at 40° angle of attack (top view).

Figure 18. Configuration B at 50° angle of attack (top view).

(a) Side view.

Figure 19. Configuration B at 55° angle of attack.

(b) Top view.
Figure 19. Concluded.

Figure 20. Configuration B at 65° angle of attack (top view).

Figure 21. Configuration B at 60° angle of attack (side view).

Figure 22. Configuration C at 30° angle of attack (top view).

Figure 23. Configuration C at 40° angle of attack (top view).

Figure 24. Configuration C at 50° angle of attack (top view).

(a) Top view.

(b) Side view.

Figure 25. Configuration C at 55° angle of attack.

Figure 26. Configuration C at 60° angle of attack (side view).

Figure 27. Configuration C at 65° angle of attack (top view).

Figure 28. Configuration D at 40° angle of attack (top view).

(a) Side view.

Figure 29. Configuration D at 55° angle of attack.

(b) Top view.

Figure 29. Concluded.

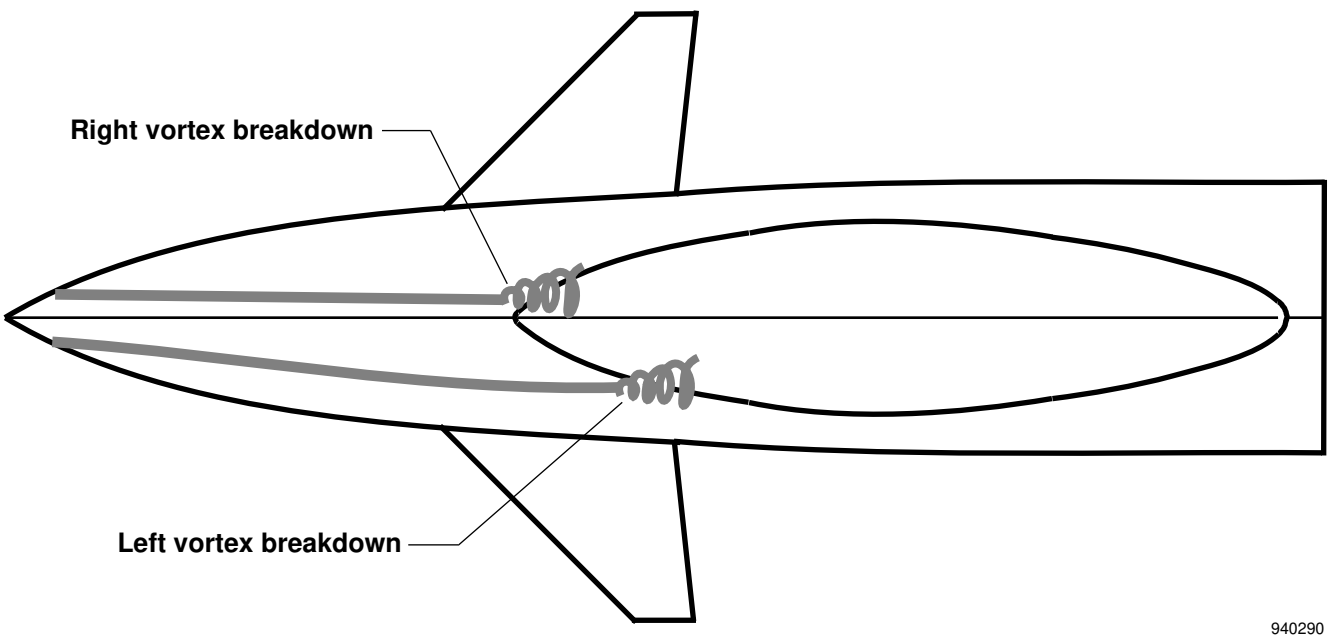

Figure 30. Primary vortex path for configuration D at 60° angle of attack.

Figure 31. Configuration E at 35° angle of attack (top view).

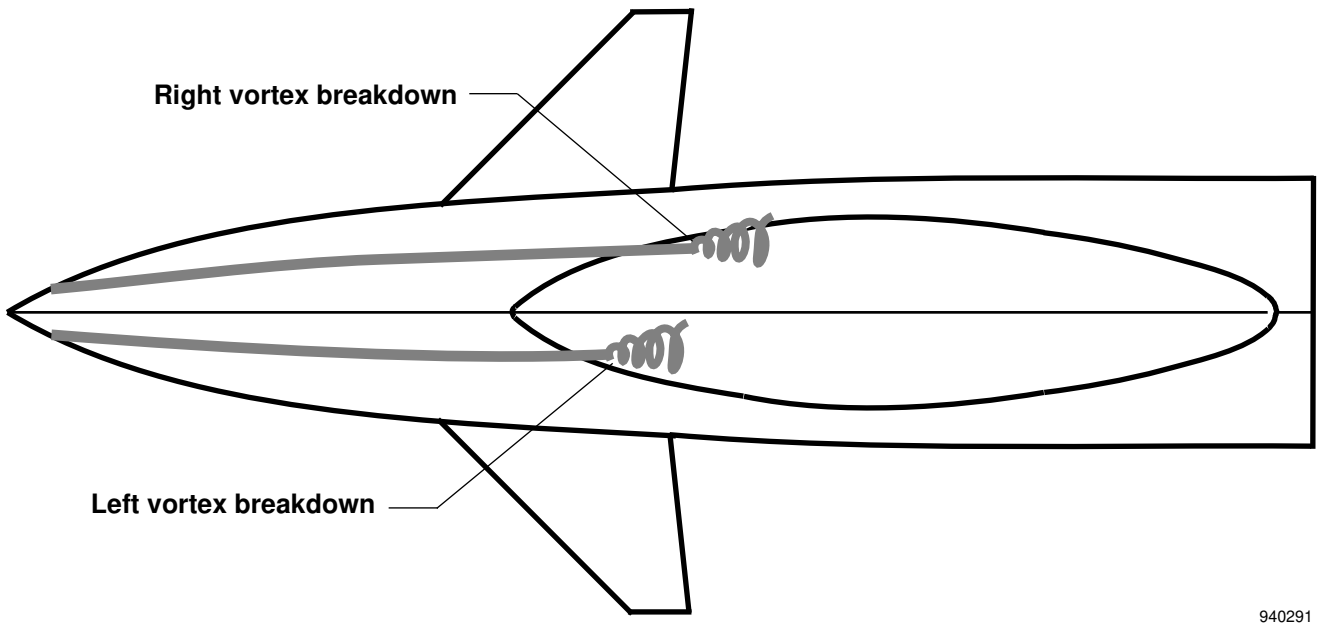

Figure 32. Primary vortex path for configuration E at 50° angle of attack.

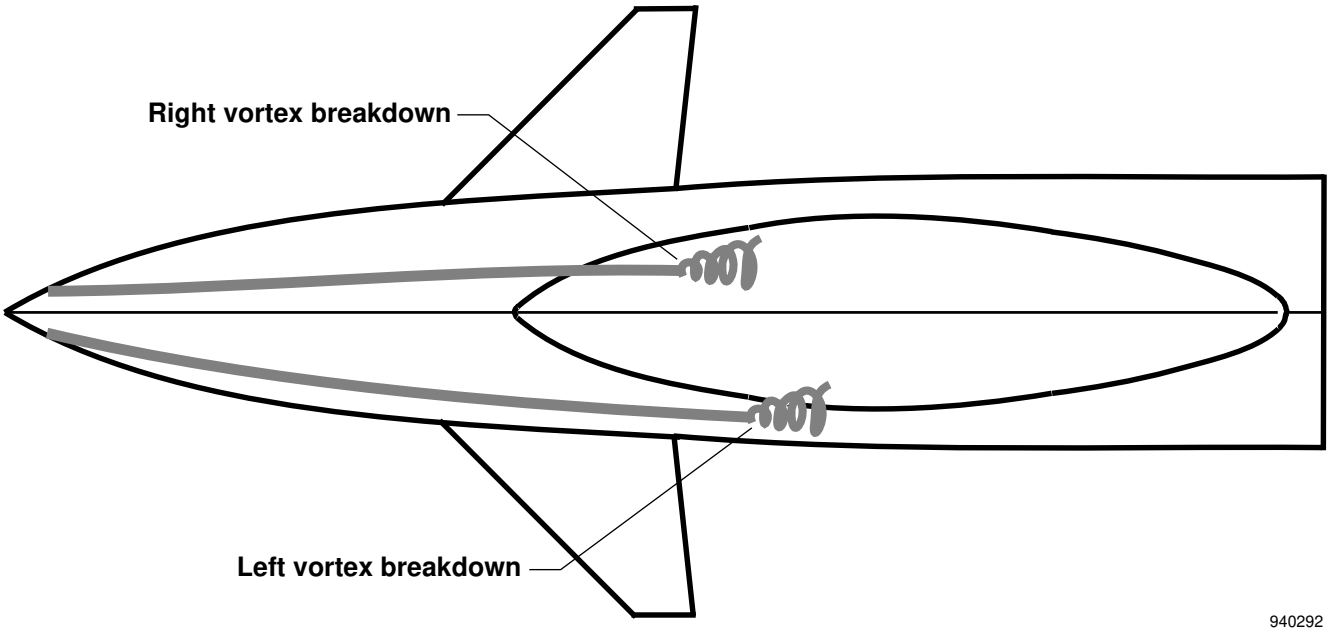

Figure 33. Primary vortex path for configuration E at 55° angle of attack.

Figure 34. Configuration F at 20° angle of attack (side view).

Figure 35. Configuration F at 40° angle of attack (top view).

Figure 36. Configuration F at 55° angle of attack (side view).

Figure 37. Configuration F at 60° angle of attack (side view).

Figure 38. Configuration F at 65° angle of attack (side view).

Figure 39. Configuration G at 40° angle of attack (top view).

Figure 40. Configuration G at 50° angle of attack (side view).

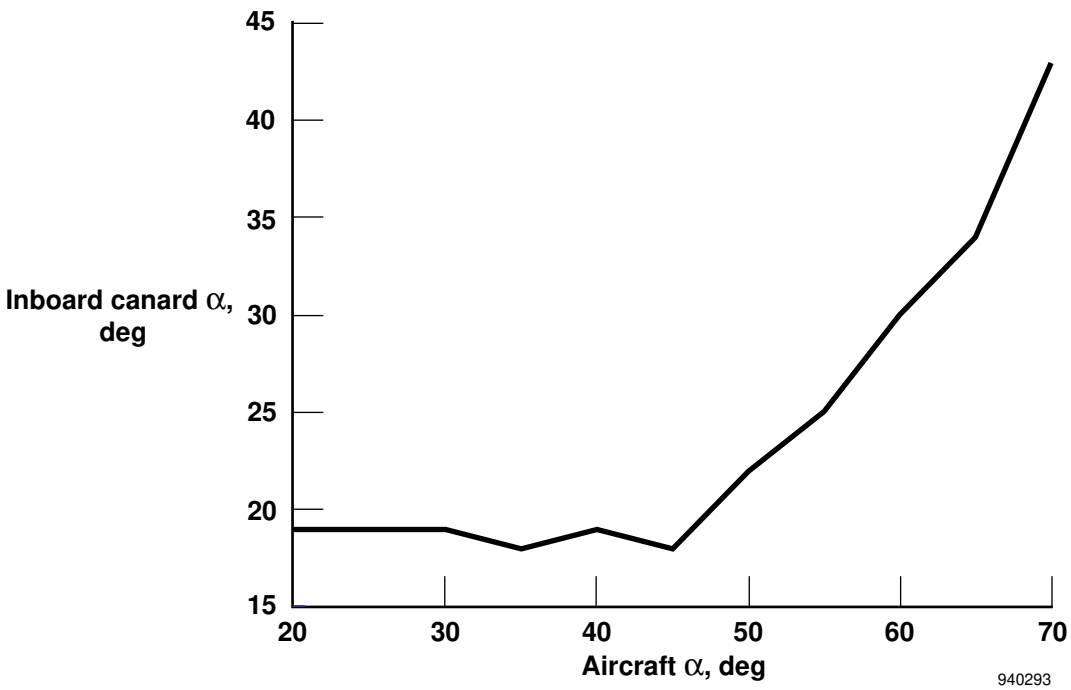

Figure 41. Local inboard canard angle of attack as a function of aircraft angle of attack (no strakes, N1 noseboom on).

Figure 42. Configuration A at 45° angle of attack (side view).

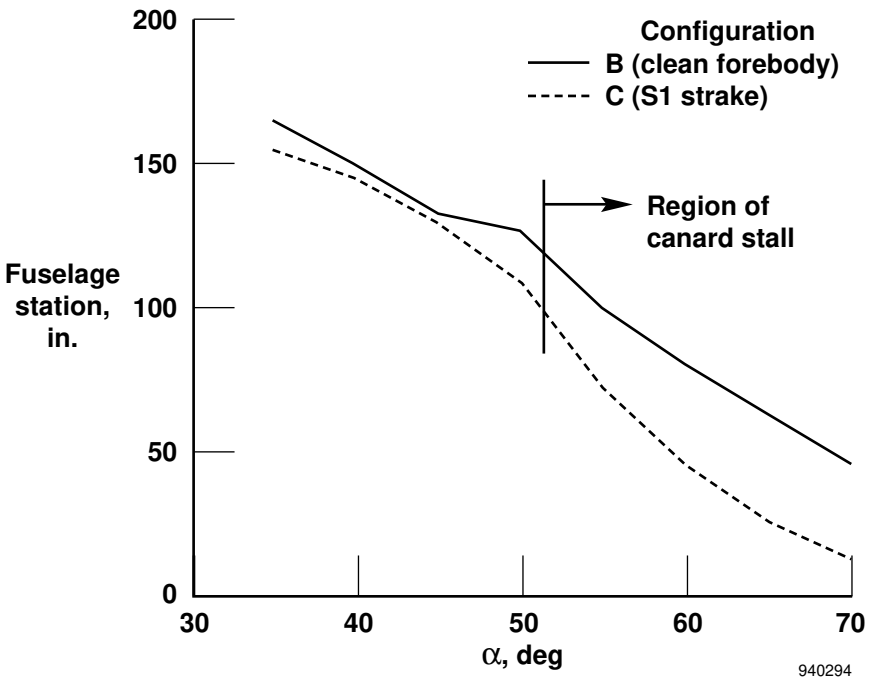

Figure 43. Comparison of primary vortex breakdown location with and without strakes.

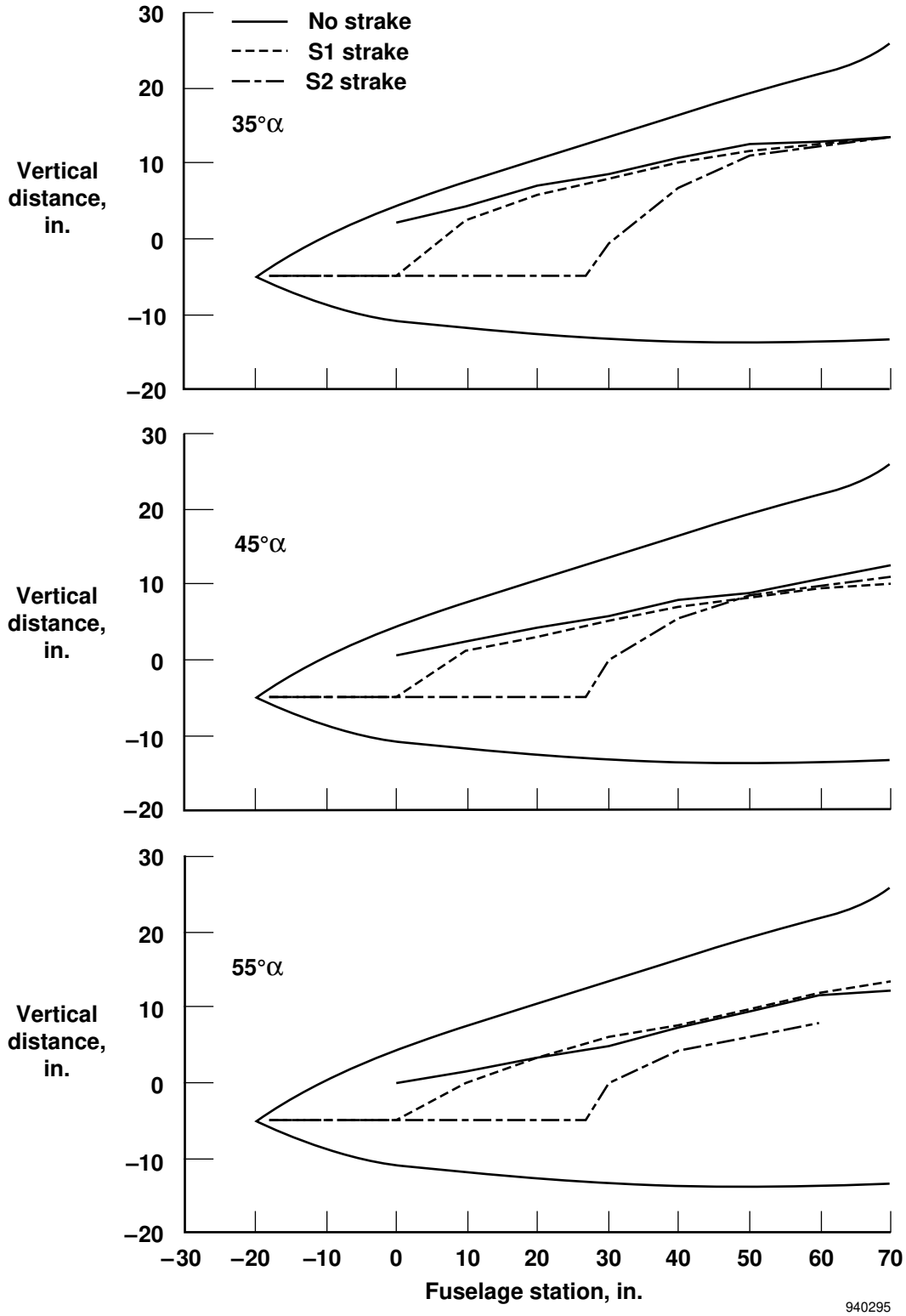

Figure 44. High-angle-of-attack primary separation line with and without strakes.

REPORT DOCUMENTATION PAGE

Form Approved
OMB No. 0704-0188

Public reporting burden for this collection of information is estimated to average 1 hour per response, including the time for reviewing instructions, searching existing data sources, gathering and maintaining the data needed, and completing and reviewing the collection of information. Send comments regarding this burden estimate or any other aspect of this collection of information, including suggestions for reducing this burden, to Washington Headquarters Services, Directorate for Information Operations and Reports, 1215 Jefferson Davis Highway, Suite 1204, Arlington, VA 22202-4302, and to the Office of Management and Budget, Paperwork Reduction Project (0704-0188), Washington, DC 20503.

1. AGENCY USE ONLY (Leave blank)	2. REPORT DATE	3. REPORT TYPE AND DATES COVERED
	September 1994	Technical Memorandum

4. TITLE AND SUBTITLE

Water Tunnel Flow Visualization Study of a 4.4% Scale X-31 Forebody

5. FUNDING NUMBERS

WU-533-02

6. AUTHOR(S)

Brent Cobleigh and John Del Frate

7. PERFORMING ORGANIZATION NAME(S) AND ADDRESS(ES)

NASA Dryden Flight Research Center
P.O. Box 273
Edwards, California 93523-0273

8. PERFORMING ORGANIZATION REPORT NUMBER

H-1997

9. SPONSORING/MONOTORING AGENCY NAME(S) AND ADDRESS(ES)

National Aeronautics and Space Administration
Washington, DC 20546-0001

10. SPONSORING/MONITORING AGENCY REPORT NUMBER

NASA TM-104276

11. SUPPLEMENTARY NOTES

12a. DISTRIBUTION/AVAILABILITY STATEMENT

Unclassified—Unlimited
Subject Category 02

12b. DISTRIBUTION CODE

13. ABSTRACT (Maximum 200 words)

A water-tunnel test of a 4.4 percent–scale, forebody-only model of the X-31 aircraft with different forebody strakes and nosebooms has been performed in the Flow Visualization Facility at the NASA Dryden Flight Research Center. The focus of the study was to determine the relative effects of the different configurations on the stability and symmetry of the high-angle-of-attack forebody vortex flow field.

The clean, noseboom-off configuration resisted the development of asymmetries in the primary vortices through 70° angle of attack. The wake of the X-31 flight test noseboom configuration significantly degraded the steadiness of the primary vortex cores and promoted asymmetries. An alternate L-shaped noseboom mounted underneath the forebody had results similar to those seen with the noseboom-off configuration, enabling stable, symmetrical vortices up to 70° angle of attack. The addition of strakes near the radome tip along the waterline increased the primary vortex strength while it simultaneously caused the vortex breakdown location to move forward. Forebody strakes did not appear to significantly reduce the asymmetries in the forebody vortex field in the presence of the flight test noseboom.

14. SUBJECT TERMS

Asymmetry; Forebody; High angle of attack; Noseboom; Strake; Vortex flow; Water tunnel; X-31

15. NUMBER OF PAGES

41

16. PRICE CODE

AO3

17. SECURITY CLASSIFICATION OF REPORT	18. SECURITY CLASSIFICATION OF THIS PAGE	19. SECURITY CLASSIFICATION OF ABSTRACT	20. LIMITATION OF ABSTRACT
Unclassified	Unclassified	Unclassified	Unlimited

NSN 7540-01-280-5500 *For sale by the National Technical Information Service, Springfield, Virginia 22161-2171* Standard Form 298 (Rev. 2-89)
Prescribed by ANSI Std. Z39-18
298-102